JMEPEG (2018) 27:1738–1745
https://doi.org/10.1007/s11665-018-3301-2

1059-9495/$19.00

Annealing Effects on Microstructure and Mechanical Properties of Ultrafine-Grained Al Composites Reinforced with Nano-Al_2O_3 by Rotary Swaging

Cunguang Chen, Wenwen Wang, Zhimeng Guo, Chunbao Sun, Alex A. Volinsky, and Vladislav Paley

(Submitted November 13, 2017; in revised form February 9, 2018; published online March 26, 2018)

Microstructure evolution and variations in mechanical properties of Al-Al_2O_3 nanocomposite produced by powder metallurgy were investigated and compared with commercially pure aluminum (Al-1050) after furnace annealing. Fine gas-atomized Al powder compacts were first sintered in flowing nitrogen, subsequently consolidated into wires by rotary swaging and eventually annealed at 300 and 500 °C for 24 h each. Scanning and transmission electron microscopy with energy-dispersive spectroscopy was utilized to document the microstructure evolution. Rotary swaging was proven to lead to a marked decrease in grain size. After heavy swaging to true deformation degree of $\varphi = 6$ and annealing at 500 °C, obvious recrystallization was observed at Al-1050's existing grain boundaries and the crystals began to grow perpendicular to the flow direction. In the Al-Al_2O_3 nanocomposite, fabricated from $d_{50} = 6$ μm Al powder, recrystallization partially occurred, while grains were still extremely fine. Due to the dual role of fine-grained Al_2O_3 dispersion strengthening, the nanocomposite showed improved mechanical performance in terms of tensile strength, approximately twice higher than Al-1050 after annealing at 500 °C.

Keywords Al composite, mechanical properties, microstructure evolution, powder metallurgy, rotary swaging

1. Introduction

In recent decades, Al powder metallurgy (PM) has become an increasingly prevalent technology in the metal manufacturing of automotive parts, wherein a balance between tight dimensional tolerances and outstanding mechanical properties is sought (Ref 1, 2). Aluminum PM is based on the large surface area of fine Al powder and introduction of naturally formed ultra-thin and dense surface oxides, which otherwise cannot be reduced into Al. Native Al_2O_3 films bring up new appealing benefits based on their superior mechanical properties, enhanced creep performance and increased thermal stability at elevated temperatures (Ref 3, 4). Based on previous studies, PM Al can be categorized into three major groups: sinter-aluminum-pulver (SAP) (Ref 3-6), SAP-like Al-AlN nanocomposite (Ref 7-15) and high-temperature aluminum (HITEMAL) (Ref 4, 6, 7, 16-18).

Generally, SAP materials consist of a broad range of oxide dispersion strengthened Al composites produced primarily from mechanically milled or further oxidized Al powders (Ref 19). However, mechanical properties of these compacts cannot be reliably reproduced because they have high production costs, problems with the elimination of the process control agent used during milling and inferior plasticity (Ref 4, 6). SAP-like Al-AlN nanocomposites are produced by replacing the native Al_2O_3 surface skin on fine Al powder with a large volume fraction of *in situ* formed nanoscale AlN dispersoids. These dispersoids are synthesized via partial nitridation of fine gas-atomized Al powder compacted in flowing nitrogen. During the fabrication process, up to 0.5 wt.% Sn powder (< 45 μm) is mixed into the fine Al powder to control the growth of the AlN layer during nitridation and avoid cracking of the green compacts (Ref 7). However, Sn is usually not evenly mixed, especially for large samples, resulting in inhomogeneous and uncontrollable formation of AlN, catastrophic overheating and cracking caused by the highly exothermic nitridation reaction. This potential risk is unsustainable in industrial production.

HITEMAL utilizes fine-grained or ultra fine-grained (UFG) Al composites reinforced with nanoscale Al_2O_3 dispersoids prepared by consolidating finely atomized Al powder via severe plastic forming (Ref 16). This Al_2O_3 phase originates from the thin (2-20 nm) oxide film present on the surface of the as-atomized powder (Ref 20). Surprisingly at a significantly lower Al_2O_3 volume (typically < 3 vol.%), HITEMAL achieves superior thermal stability and mechanical properties compared to SAP due to its unique stabilizing and strengthening effects on the submicron Al grain boundaries. Additionally, no additives are applied in the HITEMAL process like the SAP-like Al-AlN nanocomposites. Accordingly, the process is simplified, the properties are more repeatable, and the cost is decreased (Ref 7, 16).

However, survey data display that the industrial yield rate of fine gas as-atomized Al powder of commercial purity, with a mean particle size (d_{50}) of 0.5-2 μm, is statistically no more than 5 wt.%. High-quality fine Al powder must go through a special sorting process after being produced by gas-atomiza-

Cunguang Chen and **Zhimeng Guo**, Institute for Advanced Materials and Technology, University of Science and Technology Beijing, Beijing 100083, China; **Wenwen Wang**, School of Mathematics and Physics, University of Science and Technology Beijing, Beijing 100083, China; **Chunbao Sun**, School of Civil and Environmental Engineering, University of Science and Technology Beijing, Beijing 100083, China; and **Alex A. Volinsky** and **Vladislav Paley**, Department of Mechanical Engineering, University of South Florida, Tampa, FL 33620, USA. Contact e-mails: cgchen@ustb.edu.cn, wwls.wang@qq.com, and volinsky@eng.usf.edu.

tion. At present, fine Al powder with d_{50} = 0.5-2 μm can be prepared into bulk powder compacts with high performance; however, it is relatively expensive, but now available in commercial quantities (Ref 7). It should be noted that yield of gas as-atomized Al powder, in a mean size of 5-10 μm, is dramatically increased to approximately 40 wt.%. Therefore, the yield of the improved Al powder, with d_{50} = 5-10 μm, is more suitable for practical applications, since it can show excellent performance. Nevertheless, a systematic study related to characterization of powder compacts fabricated by Al powder, in the granularity range of d_{50} = 5-10 μm, does not yet exist.

Consequently, the aim of the present paper is to systematically evaluate the effects of as-atomized Al powder, with d_{50} = 6 μm, on microstructure and performance of consolidated Al materials using rotary swaging (RS) approach followed by a typical PM route (Ref 21-23). Meanwhile, combined with commercially pure (CP) aluminum, Al-1050, as well as coarser powder (d_{50} = 12 and 20 μm) compacts, the annealing evolution of microstructure and mechanical properties are investigated via scanning and transmission electron microscopy and tensile testing, respectively.

2. Experimental Procedure

Gas-atomized Al powders of technical purity (99.8%) with an average size of 6, 12 and 20 μm (Al-6, Al-12, Al-20, respectively, supplied by the Angang Group Aluminum Powder Co., Ltd., China), and CP Al-1050 with a chemical composition of Fe 0.142 wt.%, Si 0.105 wt.%, Mn 0.064 wt.%, Ti 0.015 wt.%, Zn 0.013 wt.%, V 0.01 wt.%, Mg 0.028 wt.% and Al balance, were received as hot extruded bars. Initially, loose Al powder was cold isostatically pressed (CIP) at 180 MPa with vacuum assistance prior to consolidation. As proven by the Archimedes density measurements, the relative density of CIP powder was about 86% of the theoretical density (THD). The resulting green bodies (Φ 70 mm × 300 mm) were then compacted by nitrogen activated sintering in an alumina tube furnace, which was evacuated to 10 Pa after placing the samples. Nitrogen gas (99.999% pure) was introduced at a flow rate of 1 L min^{-1}, and the samples were directly heated to 610 °C at 5 °C min^{-1} for 180 min of nitridation.

Subsequently, RS of PM Al was completed in an effort to simulate the effects of hot forging. This process used an alternating blow swagger with a four-die arrangement. Swaging was performed on sintered cylindrical bars that were fully machined to achieve the required dimensional tolerances (Φ 20 mm × 100 mm) as well as Al-1050 bars. Various deformation degrees were applied at room temperature. Deformation degree (φ) was calculated as $\varphi = \ln(A_0/A)$, where A_0 is the initial cross section and A is the final cross section. A stationary spindle swaging machine was obtained from the Xi'an Innovation Precision Instrument Research Institute, China (Ref 24). The principle of its operation was previously reported in references (Ref 21 and 23). The rod samples were heated to 480 °C and held for 10 min before each swaging deformation with $\varphi < 0.52$. However, the samples were swaged out at room temperature when $\varphi > 0.52$. A set of molds was used to reduce the size of the work piece from Φ 20 mm to Φ 1 mm. Various conditions studied are listed in Table 1. Due to the large deformation from Φ 20 mm to Φ 5.6 mm, the stress concentration on the sample surface and poor plasticity caused peeling and cracking. Therefore, an annealing process at 400 °C for 60 min was conducted in order to relieve the stress of the sample S7. In order to study the thermal stability of the swaged materials, air annealing at 300 °C for 24 h and 500 °C for 24 h was conducted. Comparatively, the same treatment of Al-1050 was carried out as well.

Microstructure examinations of sintered and swaged samples were carried out using scanning electron microscopy (SEM, LEO 1450, Carl-Zeiss Company), field-emission scanning electron microscopy (FE-SEM, SUPRA 55, Carl-Zeiss Company) and transmission electron microscopy (TEM, Tecnai G2 F30, FEI Company) equipped with energy-dispersive x-ray spectroscopy (EDS). To clearly demonstrate the presence and distribution of nanometric oxide dispersoids, samples for TEM observations were prepared by electro-etching, followed by ion polishing applied for a short time. Such treated samples featured oxide dispersoids that tiled and protruded over the etched Al matrix surface, which was beneficial for easier localization. Mechanical properties of the swaged and annealed Al wires were measured using tensile specimens with a gauge of Φ1 × 50 mm directly cut from the S15 sample. The tensile tests were performed at room temperature with a crosshead speed of 0.5 mm min^{-1}. Each set of data reported was based on the properties obtained from 3 to 5 samples.

3. Results and Discussion

3.1 Microstructure of Consolidated Al Composites

To verify that the PM processed bars were sintered in a manner consistent with prior findings, the sintered density and microstructure of as-sintered materials were assessed. As measured, the cylinders made of Al-20, Al-12 and Al-6 achieved 97.6, 98.5 and 99.2% of the aluminum THD, respectively. The as-sintered microstructure of PM pure Al is shown in Fig. 1. Previous work displayed the Al-1050 microstructure in the as-received condition with relatively coarse grains (∼ 150 μm seen from Fig. 1d), while Fig. 1 shows the sintered microstructures of the PM pure Al with a grain size of 5-20 μm, retaining the initial spherical shape of the gas-atomized powder particles. Regardless of the Al powder granularity, the prior particle boundaries (PPBs) in the sintered microstructure are visible in Fig. 1(a), (b) and (c). The white phases along the PPBs are regarded as Al_2O_3 derived from the Al powder skin via the EDS analysis. It is known from previous results that severe deformation, such as quasi-isostatic forging and extrusion, can be chosen for breaking up the PPBs, thus enhancing ductility and toughness (Ref 25).

The presence of pores in the sintered Al is seen in the micrograph as the black regions with white margin. It is clear that the diameter of the pores gets smaller as the size of the Al powder particles decreases. As indicated from the basal principle, the finer the powder particles, the larger the specific surface area and the intrinsic surface driving force. Accordingly, the sintered densification of the Al-6 compact can be significantly improved due to the effect of nitrogen activated sintering. The appreciable densification of the PM specimens is consistent with the high sintered density observed in previous reports (Ref 3, 7, 26). Although the PM pure Al-6 is very dense, even a small quantity of pores can have negative effects (Ref

Table 1 Deformation degree of the swaged samples

Sample	Diameter, mm	True strain	Swaging temperature, °C
S0	20	0	480
S1	17.2	0.3	
S2	15.4	0.52	
S3	14.5	0.64	Room temperature
S4	12.4	0.96	
S5	9.7	1.45	
S6	8.1	1.81	
S7	5.6	2.55	
S8	4.3	3.07	
S9	3.9	3.27	
S10	3	3.79	
S11	2.7	4	
S12	2.4	4.24	
S13	1.7	4.93	
S14	1.4	5.32	
S15	1	6	

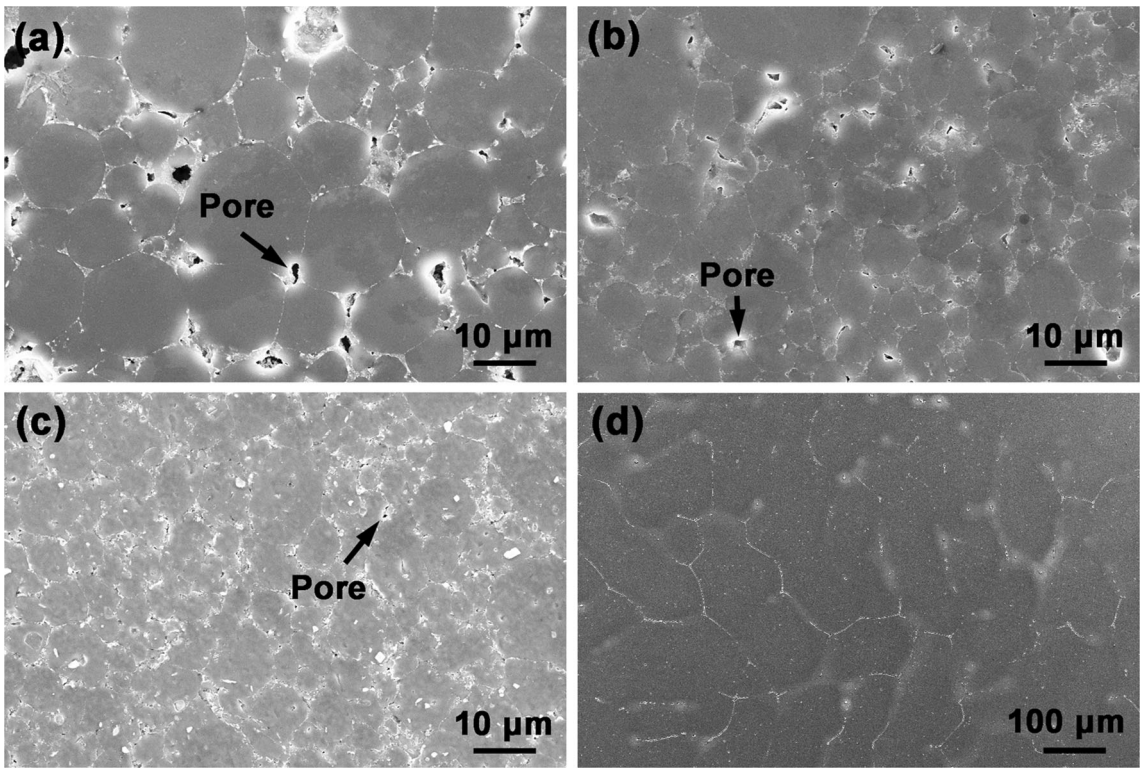

Fig. 1 SEM images of as-sintered PM pure Al samples with (a) d_{50} = 20 μm, (b) d_{50} = 12 μm, (c) d_{50} = 6 μm Al powder and (d) as-received Al-1050

27). The complete elimination of this attribute is central to all PM forging processes, and likewise, critical to this study as well. However, the Al-1050 microstructure differs considerably. For one, there is no observable amount of pores present. Another is the presence of the dispersoid phase in Al-1050 seemingly absent from the PM system.

3.2 Swaged and Annealed Microstructure Observations

To further improve the sintered properties, RS modifications to the microstructure were considered. To assess the microstructure distinction of the thermal stability between the PM and commercially pure Al, annealing at 300 and 500 °C was completed afterwards. The as-swaged and as-annealed TEM microstructure of both Al-6 and Al-1050 wires is shown in Fig. 2. The examples of the resultant TEM micrographs are displayed for the S15 samples deformed with $\varphi = 6$. Examination of the swaged wires shows deformation and fragmentation of the initial powder particles into elongated grains, primarily aligned along the swaging direction. The transverse grain size of the swaged powder compacts is ~ 0.5 μm, about half the size of the Al-1050 grains under the same deformation conditions, as shown in Fig. 2(a) and (b).

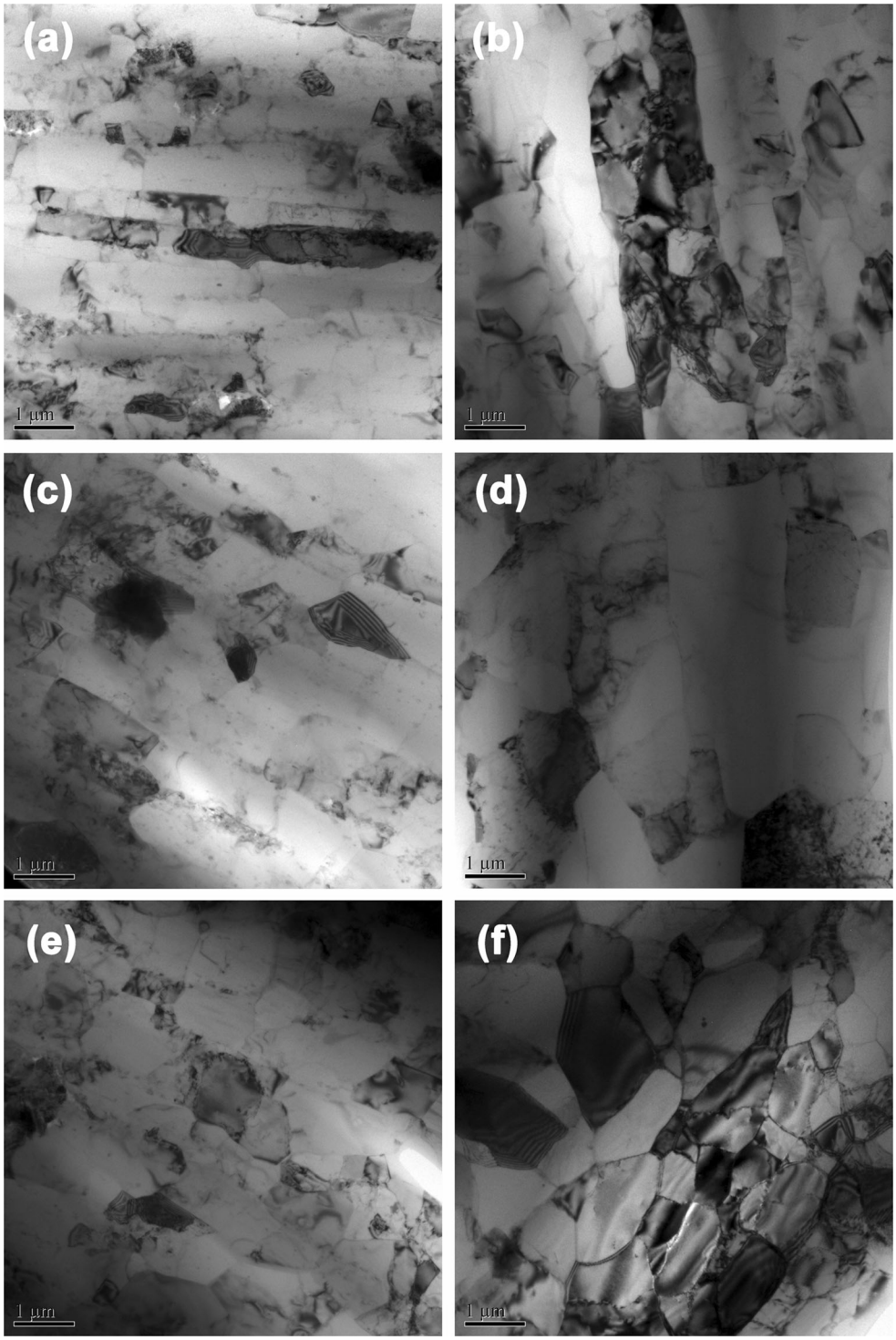

Fig. 2 Bright field TEM images parallel to the swaging direction of Φ1 mm wire samples: (a) as-swaged Al-6, (b) as-swaged Al-1050, (c) as-annealed Al-6 at 300 °C, (d) as-annealed Al-1050 at 300 °C, (e) as-annealed Al-6 at 500 °C and (f) as-annealed Al-1050 at 500 °C

After the annealing treatment at 300 °C for 24 h, Al-6 compacts showed slightly coarser microstructure, as seen in Fig. 2(c), and a transverse grain size of ∼ 1 μm. It was also vaguely seen that a few subgrain boundaries exist within the elongated grains, that is, subgrains have started to develop in the process of intermediate temperature annealing. Regarding the microstructure changes of Al-1050, although the strips morphology can still be observed in Fig. 2(d), the grain size along the width direction is ∼ 2 μm. Meanwhile, it can be clearly recognized that the structure consisted of blocky subgrains with a higher dislocation density and subgrain boundaries made up of dislocation tangles. From reference (Ref 28), which refers to the recovery mechanism of pure Al cold deformation, it can be inferred that the microstructure of

the Al-1050 annealed sample has transferred from the recovery stage to the recrystallization stage, while the recovery of the Al-6 annealed wires still happened continually.

Despite minor grain growth attributed to extreme annealing at 500 °C for 24 h, as shown in Fig. 2(e), elongated grains of the Al-6 sample are evolved into the distinct cystiform microstructure accompanied by a low dislocation density. It is indicated that the recrystallization of Al-6 has not yet occurred. This is similar to the high Al_2O_3 content SAP materials studied by Hansen (Ref 29) and Balog (Ref 6). Comparatively, the major microstructure alterations are observed in the Al-1050 sample, as seen in Fig. 2(d). Further elevation of annealing temperature to 500 °C activates growth of fragmented subgrains produced previously and their recrystallization into polygonal grains. Consequently, the different characteristics of the microstructure experienced at 300 and 500 °C annealing treatment exhibit that the complete recrystallization temperature of PM swaged Al is improved at 500 °C.

Now that both research objects in this study are pure Al, no matter how they were prepared, a few precipitation phases introduced by impurity elements, such as Fe and Si, should have very limited positive influence on microstructure evolution in the annealing process. The impurities can be dissolved at high temperature, especially at 500 °C, and slowly reprecipitate out and coarsen during the annealing process. However, naturally formed nanoscale Al_2O_3 on the surface of the Al powder is hard to eliminate. It should be pointed out that the Al_2O_3 is thermodynamically stable at ~ 500 °C. Even if the amount of nano-Al_2O_3 is very small, which is expected to act as obstacles for dislocation slip (Orowan strengthening) and grain boundary migration, it can lead to a significant difference in microstructure and mechanical properties. Further details on the effects of nano-Al_2O_3 are provided later in this study.

3.3 Effects of RS and Annealing on Nano-Al_2O_3

TEM observations (Fig. 3a) reveal relatively uniform distribution of nano-Al_2O_3 (dark in contrast) dispersoids along the grain boundaries and inside the grain of the Al-6 swaged wire with $\varphi = 6$. On the other hand, an Al_2O_3 particle with ~ 15 nm size is detected in the high-resolution TEM (HR-TEM) image (Fig. 3b). It was previously found that the dispersoids were α-Al_2O_3 (Ref 30) and shear deformation induced during extrusion fractured the native oxide layer into separate plate-like dispersoids (Ref 6). However, as seen in the figure, Al_2O_3 particles embedded in the Al matrix are more irregular than lamellate.

High deformation energy induced by RS yielded finer microstructure with some of the broken oxides found within newly arising grains, as seen in Fig. 3(c). In Fig. 3(d), the interaction trace of Al_2O_3 particles with the dislocation can be clearly observed at high magnification. The Al_2O_3 dispersoids inside the grain are further ascertained by the TEM-EDS results in Fig. 4. This is the unique and interesting first time discovery, which is not directly given in any other relevant research report.

Figure 5 shows the TEM images parallel to the swaging direction of the Al-6 swaged and annealed samples with $\varphi = 6$ (Φ 1 mm wires). Granular Al_2O_3 oxide particles are homogenously redistributed within compacts with predominant position along the grain boundaries (i.e., initial powder surface). Nanoscale dispersions effectively pin microstructure, yielding excellent structural stability with no detected dramatic structural changes observed after 24-h annealing at 350 °C. Even after extreme annealing at 500 °C for 24 h, minor grain growth is accompanied with spheroidization (minimization of surface energy) of oxide particles. It is worth noting that at elevated temperatures, there is no apparent change in the size of Al_2O_3 dispersoids, most of which stay at 10-50 nm. These results are in agreement with the microstructure in Fig. 2 and have also been discussed similarly in the extrusion microstructure after severe exposure at 500 °C for 24 h described in previous work (Ref 6, 30).

3.4 Mechanical Properties

Figure 6 presents the dependence of the yield strength (YS), ultimate tensile strength (UTS) and elongation to fracture on the treatment temperatures induced in Φ 1 mm wires of Al-6 and Al-1050 during RS and annealing. Taking the difference between YS and UTS (i.e., yield ratio) as a coarse measurement of work hardening capability, it is seen that this value for the as-swaged materials is very close to 1. As shown in Fig. 6(a) and (b), YS and UTS of the PM Al-6 are superior to Al-1050 after the swaging process by a factor of 6, whereas the performance of other two kinds of swaged samples, prepared by Al-12 and Al-20 powder, is inferior to Al-1050. High strength values of compacts by PM in contrast to contemporary Al-1050 work hardening reflect three major distinct strengthening mechanisms. For one, fine nature of as-atomized powder results in a high amount of grain boundaries within compacts, which give a rise to the predominant effect of grain boundary strengthening. Since the grain size of metals is reduced, YS increases. As presented by the swaged data, the finer the Al powder, the smaller the grain size became, and higher strength was exhibited. For another, remarkable influence of the Orowan strengthening mechanism is active, in the case of those Al-6 compacts where oxide particles were embedded within the grain areas, as seen in Fig. 3(a) and (d). However, it may be due to a handful of oxides on the skin of the coarser Al powder, such as Al-12 and Al-20, that the marginal effect on the tensile performance is reflected, compared to the Al-6 wire in Fig. 6(a) and (b). In addition, one factor is the obvious removal of residual porosity given that this feature is known to have a damaging effect on all tensile properties. The fully dense product would have then performed as a metal matrix composite to offer better YS and UTS compared with the Al-1050 material.

It was also discovered that the strength of the as-swaged Al-6 wires gradually declines with increasing annealing temperature as the contribution from individual strengthening mechanisms reduces. This can be accounted for by the Orowan strengthening mechanism. In this case, at 500 °C annealing temperature, the shape of the Al_2O_3 dispersoids transforms from an irregular shape to a spherical shape and the dispersions interval increases. The Orowan relationship between the yield stress and particles interval is $\tau_c = Gb/\lambda$, where τ_c denotes the critical shear stress equal to the yield stress, λ represents the particles interval along the dislocation line, G is the shear modulus, and b is the Burger's vector. It can be concluded that the yield stress is inversely proportional to the particles' interval, indicating that the expanded spacing variation of the dispersions is accompanied by further strength deterioration. The experimental result in Fig. 5 was consistent with the Orowan relationship. Nano-Al_2O_3 particles interval widened at higher annealing temperature from ~ 100 nm as-swaged in Fig. 5(a) to ~ 200 nm as-annealed at 500 °C in Fig. 5(c),

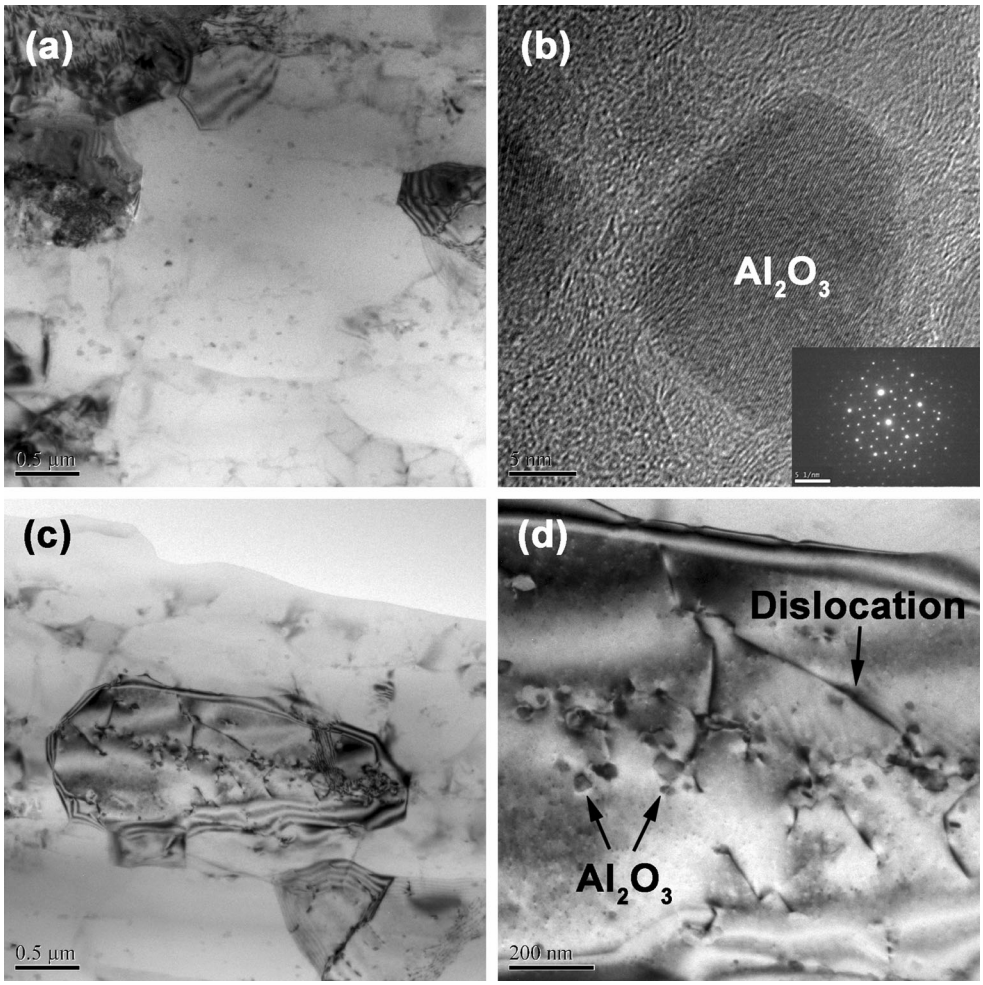

Fig. 3 Bright field TEM images parallel to the swaging direction of Φ1 mm wire sample of as-swaged Al-6, showing (a) uniform distribution of nano-Al_2O_3 (dark in contrast) dispersoids, (b) HR-TEM image of Al_2O_3, (c) newly arising grains including broken oxides inside and (d) the interaction trace of Al_2O_3 particles with the dislocation. The bottom right corner in (b) is the corresponding diffraction pattern image from Al_2O_3 nanoparticles

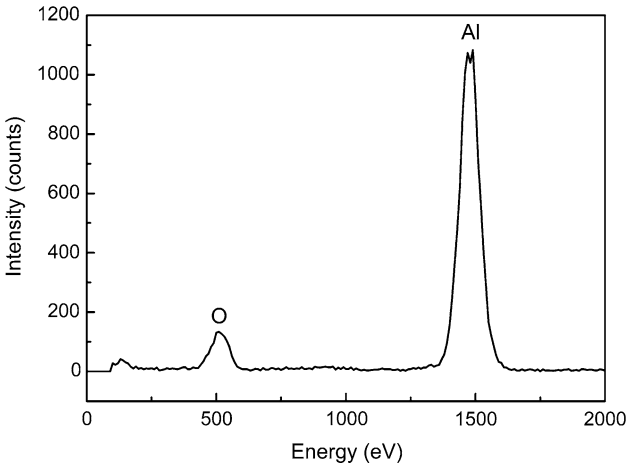

Fig. 4 TEM-EDS spectra of dispersoids in the Al-6 matrix

while the YS dropped from 181 to 87 MPa correspondingly seen from Fig. 6(a). That is, when the nanoparticles interval doubled, the YS more or less halved. The second factor pertains to slight grain growth observed from a combination of Fig. 2(a), (c), and (e), after 300 and 500 °C annealing, which resulted in decreased strength.

Most importantly, both YS and UTS of the Al-1050 swaged wire decrease dramatically just after 300 °C annealing, but the elongation to fracture increases sharply from as-swaged 14.7-46% after 500 °C annealing. As for the compacts by PM, the elongation to fracture drops as the Al powder particle size decreases, but increases with testing temperature. This finding is unlike other studies showing reduced fracture resistance at elevated temperatures, which is attributed to strain localization and plastic instability between growing microvoids (Ref 6). Significantly lower ductility of RS prepared compacts by Al-6 powder (∼ 1.6%) can be attributed to disadvantageous texture of elongated grains. Since the reduced ductility is explained by dynamic recovery, theories based on the work hardening dislocation cell, and source structures in submicron grains, are no longer applicable. Besides, similar to porosity, Al_2O_3 dispersoids in the form of ceramic addition present in the product are also known to reduce tensile ductility. With respect to the Al-1050 material, except for the effect of work hardening, no other effective strengthening sources, apart from the limited impurity precipitation phases, can conduce to the rather high strength induced by RS. Moreover, massive

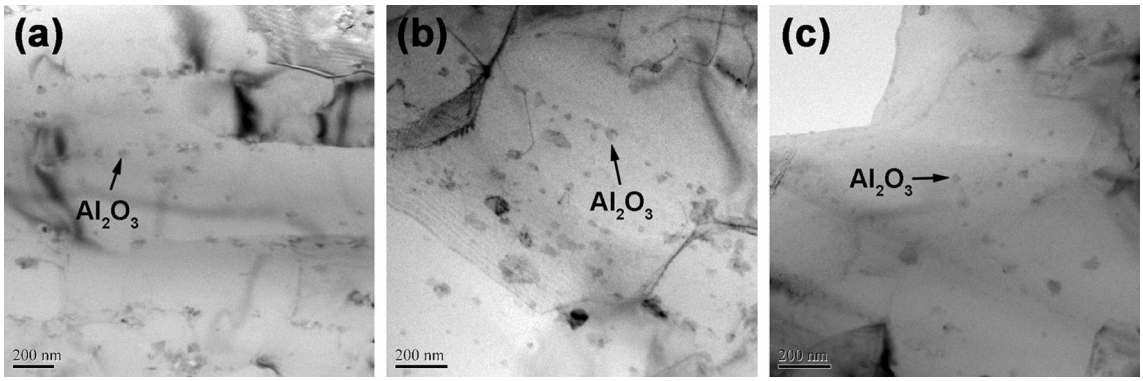

Fig. 5 Bright field TEM images parallel to the swaging direction of Φ1 mm wire samples: (a) as-swaged and as-annealed Al-6 (b) at 300 °C and (c) at 500 °C for 24 h. The black arrows indicate morphology features of native Al_2O_3 with annealing temperature elevation

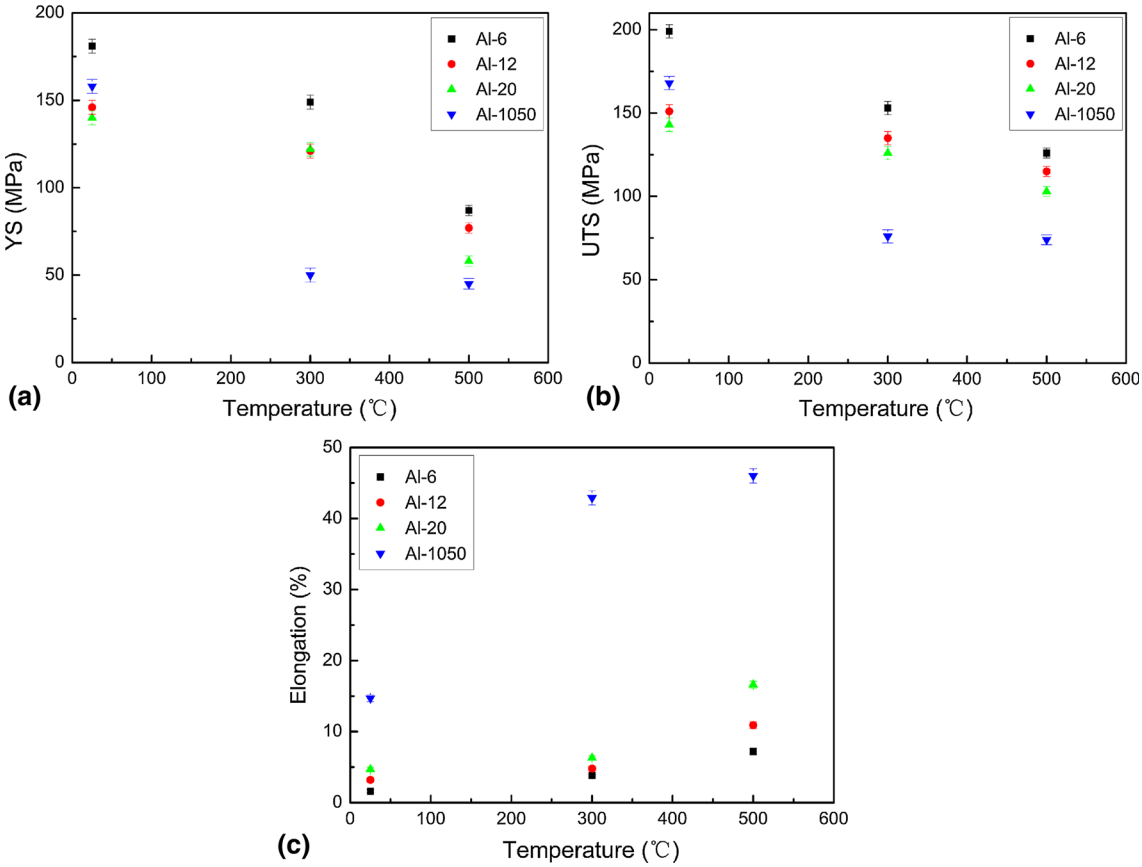

Fig. 6 Tensile properties of as-swaged and as-annealed Φ1 mm Al wire samples measured at room temperature (RT): (a) YS—the yield tensile strength, (b) UTS—the ultimate tensile strength and (c) elongation to fracture. Al-6, Al-12, Al-20 and Al-1050 represent PM pure Al wire samples with d_{50} = 6, 12 and 20 μm Al powder and commercially pure Al wire sample, respectively

recrystallization and grain growth afterwards during the annealing treatment reduce its mechanical properties.

4. Conclusions

A novel class of UFG Al-Al_2O_3 nanocomposites taken for HITEMAL has been fabricated via RS followed by a typical Al PM route with a high yield of fine gas-atomized Al powder (d_{50} = 6 μm). The annealing effects on microstructure evolution and mechanical properties were investigated. The following findings were made.

- The sintered densification of fine Al powder (d_{50} = 6 μm) can be readily obtained at 610 °C in flowing nitrogen at atmospheric pressure.
- After RS, with severe deformation of φ = 6, the oxide layer on each fine Al powder particle is largely dispersed along the grain boundaries and partially embedded inside the grains in the form of Al_2O_3 nanocrystals, yielding a dual mechanism consisting of grain refinement strengthen-

ing and nanoscale Al_2O_3 dispersion strengthening (Orowan).

- The annealing microstructure of the powder compacts made from gas-atomized Al powder (d_{50} = 6 μm) is distinct from the Al-1050 counterpart. After annealing at 500 °C, the Al-6 swaged wire, parallel to the swaging direction, retains fine grains with partial recrystallization, whereas Al-1050 has absolutely completed recrystallization and the grains have sharply grown.
- The small volume fraction of the native Al_2O_3 dispersoids, stable at elevated temperatures, results in a largely improved tensile strength, approximately twice higher than commercially pure Al-1050 after annealing at 500 °C.

Acknowledgments

This work was supported by the Fundamental Research Funds for the Central Universities (Grant No. FRF-TP-16-017A1) and the National High Technology Research and Development Program of China (Grant No. 2013AA031104).

References

1. C.D. Boland, R.L. Hexemer, Jr., I.W. Donaldson, and D.P. Bishop, Industrial Processing of a Novel Al-Cu-Mg Powder Metallurgy Alloy, *Mater. Sci. Eng., A*, 2013, **559**, p 902–908
2. R.E.D. Mann, R.L. Hexemer, Jr., I.W. Donaldson, and D.P. Bishop, Hot Deformation of an Al-Cu-Mg Powder Metallurgy Alloy, *Mater. Sci. Eng., A*, 2011, **528**, p 5476–5483
3. P. Krizik, M. Balog, E. Illekova, P. Svec, Sr, I. Matko, M. Stepnek, M. Nosko, and F. Simancik, The Oxidation Behavior of Gas-atomized Al and Al Alloy Powder Green Compacts During Heating before Hot Extrusion and the Suggested Heating Process, *J. Mater. Process. Technol.*, 2014, **214**, p 1165–1172
4. M. Balog, C. Poletti, F. Simancik, M. Walcher, and W. Rajner, The Effect of Native Al_2O_3 Skin Disruption on Properties of Fine Al Powder Compacts, *J. Alloys Compd.*, 2011, **509S**, p S235–S238
5. R. Irman, Sintered Aluminium with High Strength at Elevated Temperatures, *Metallurgia*, 1952, **46**, p 125–133
6. M. Balog, F. Simancik, M. Walcher, W. Rajner, and C. Poletti, Extruded Al-Al_2O_3 Composites Formed in Situ during Consolidation of Ultrafine Al Powders: Effect of the Powder Surface Area, *Mater. Sci. Eng., A*, 2011, **529**, p 131–137
7. M. Balog, P. Krizik, M. Yan, F. Simancik, G.B. Schaffer, and M. Qian, SAP-Like Ultrafine-grained Al Composites Dispersion Strengthened with Nanometric AlN, *Mater. Sci. Eng., A*, 2013, **588**, p 181–187
8. K. Kondoh, A. Kimura, and R. Watanabe, Effect of Mg on Sintering Phenomenon of Aluminium Alloy Powder Particle, *Powder Metall.*, 2001, **44**, p 161–164
9. Q. Hou, R. Mutharasan, and M. Koczak, Feasibility of Aluminium Nitride Formation in Aluminum Alloys, *Mater. Sci. Eng., A*, 1995, **195**, p 121–129
10. T.B. Sercombe and G.B. Schaffer, On the Role of Tin in the Nitridation of Aluminium Powder, *Scripta Mater.*, 2006, **55**, p 323–326
11. T.B. Sercombe and G.B. Schaffer, On the Role of Tin in the Infiltration of Aluminium by Aluminium for Rapid Prototyping Applications, *Scripta Mater.*, 2004, **51**, p 905–908
12. P. Yu, M. Balog, M. Yan, and G.B. Schaffer, *In situ* Fabrication and Mechanical Properties of Al-AlN Composite by Hot Extrusion of Partially Nitrided AA6061 Powder, *J. Mater. Res.*, 2011, **26**, p 1719–1725
13. M. Balog, P. Yu, M. Qian, M. Behulova, P. Svec Sr, and R. Cicka, Nanoscaled Al-AlN Composites Consolidated by Equal Channel Angular Pressing (ECAP) of Partially in situ Nitride Al Powder, *Mater. Sci. Eng., A*, 2013, **562**, p 190–195
14. D. Kent, G.B. Schaffer, T.B. Sercombe, and J. Drennan, A Novel Method for the Production of Aluminium Nitride, *Scripta Mater.*, 2006, **54**, p 2125–2129
15. W.W. Yang, Z.M. Guo, L.C. Guo, H.Q. Cao, J. Luo, and A.P. Ye, *In situ* Fabrication and Properties of AlN Dispersion Strengthened 2024 Aluminum Alloy, *Int. J. Miner. Metall. Mater.*, 2014, **21**, p 1228–1232
16. M. Balog, P. Krizik, M. Nosko, Z. Hajovska, M.V.C. Riglos, W. Rajner, D.S. Liu, and F. Simancik, Forged HITEMAL: Al-based MMCs Strengthened with Nanometric Thick Al_2O_3 Skeleton, *Mater. Sci. Eng., A*, 2014, **613**, p 82–90
17. M. Cavojsky, M. Balog, J. Dvorak, E. Illekova, P. Svec, P. Krizik, D. Janickovic, and F. Simancik, Microstructure and Properties of Extruded Rapidly Solidified $AlCr_{4.7}Fe_{1.1}Si_{0.3}$ (at.%) Alloys, *Mater. Sci. Eng., A*, 2012, **549**, p 233–241
18. C. Poletti, M. Balog, F. Simancik, and H.P. Degischer, High-Temperature Strength of Compacted Submicrometer Aluminium Powder, *Acta Mater.*, 2010, **58**, p 3781–3789
19. N. Guo, B. Luan, F. He, Z. Li, and Q. Liu, Influence of Flake Thickness on the Shape and Distribution of Al_2O_3 Particles in Al Matrix Composites Fabricated by Flake Powder Metallurgy, *Scripta Mater.*, 2014, **78–79**, p 1–4
20. C.G. Chen, L.C. Guo, J. Luo, J.J. Hao, Z.M. Guo, and A.A. Volinsky, Aluminum Powder Size and Microstructure Effects on Properties of Boron Nitride Reinforced Aluminum Matrix Composites Fabricated by Semi-Solid Powder Metallurgy, *Mater. Sci. Eng., A*, 2015, **646**, p 306–314
21. M.A. Abdulstaar, E.A. El-Danaf, N.S. Waluyo, and L. Wagner, Severe Plastic Deformation of Commercial Purity Aluminum by Rotary Swaging: Microstructure Evolution and Mechanical Properties, *Mater. Sci. Eng., A*, 2013, **565**, p 351–358
22. M. Abdulstaar, M. Mhaede, L. Wagner, and M. Wollmann, Corrosion Behaviour of Al 1050 Severely Deformed by Rotary Swaging, *Mater. Des.*, 2014, **57**, p 325–329
23. W.M. Gan, Y.D. Huang, R. Wang, G.F. Wang, A. Srinivasan, H.G. Brokmeier, N. Schell, K.U. Kainer, and N. Hort, Microstructures and Mechanical Properties of Pure Mg Processed by Rotary Swaging, *Mater. Des.*, 2014, **63**, p 83–88
24. Q. Zhang, K.Q. Jin, D. Mu, P.J. Ma, and J. Tian, Rotary Swaging Forming Process of Tube Workpieces, *Procedia Eng.*, 2014, **81**, p 2336–2341
25. T.D. Topping, B. Ahn, Y. Li, S.R. Nutt, and E.J. Lavernia, Influence of Process Parameters on the Mechanical Behaviour of an Ultrafine-Grained Al Alloy, *Metall. Mater. Trans. A*, 2012, **43A**, p 505–519
26. G.B. Schaffer and B.J. Hall, The Influence of the Atmosphere on the Sintering of Aluminum, *Metall. Mater. Trans. A*, 2002, **33A**, p 3279–3284
27. R.J. Dashwood and G.B. Schaffer, Powder Forging of a Sintered Al-3.8Cu-1 Mg-0.8Si-0.1Sn Alloy, *Mater. Sci. Eng., A*, 2002, **323**, p 206–212
28. H. Jazaeri and F.J. Humphreys, The Transition from Discontinuous to Continuous Recrystallization in Some Aluminium Alloys—Annealing Behaviour, *Acta Mater.*, 2004, **52**, p 3251–3262
29. N. Hansen, Dispersion Strengthened Aluminium Powder Products for Nuclear Application, *Powder Metall.*, 1967, **10**, p 94
30. B. Martin, S. Frantisek, B. Otto, and G. Requena, ECAP vs. Direct Extrusion—Techniques for Consolidation of Ultra-Fine Al Particles, *Mater. Sci. Eng., A*, 2009, **504**, p 1–7